Polysaccharide breakdown products drive degradation-dispersal cycles of foraging bacteria through changes in metabolism and motility

Astrid KM Stubbusch[1,2,3], Johannes M. Keegstra[4], Julia Schwartzman[5,6], Sammy Pontrelli[7], Estelle E. Clerc[4], Roman Stocker[4], Cara Magnabosco[3], Olga T. Schubert[1,2], Martin Ackermann[1,2,8], Glen G D'Souza[1,2]

[1]Institute of Biogeochemistry and Pollutant Dynamics, Department of Environmental Systems Science, ETH Zurich, Zurich, Switzerland
[2]Department of Environmental Microbiology, Eawag: Swiss Federal Institute of Aquatic Science and Technology, Duebendorf, Switzerland
[3]Geological Institute, Department of Earth Sciences, ETH Zurich, Zurich, Switzerland
[4]Institute of Environmental Engineering, Department of Civil, Environmental and Geomatic Engineering, ETH Zurich, Zurich, Switzerland
[5]Department of Civil and Environmental Engineering, MIT, Cambridge, MA, USA
[6]Department of Biology, University of Southern California, Los Angeles, USA
[7]Institute of Molecular Systems Biology, Department of Biology, ETH Zurich, Zurich, Switzerland
[8]Laboratory of Microbial Systems Ecology, School of Architecture, Civil and Environmental Engineering (ENAC), École Polytechnique Fédéral de Lausanne (EPFL), Lausanne, Switzerland

ORCID:
GD: 0000-0002-9123-101X
AS: 0000-0003-4767-2712
JK: 0000-0002-8877-4881
JS: 0000-0003-4563-4835
EC: 0009-0003-6046-2856
SP: 0000-0001-6265-8842
RS: 0000-0002-3199-0508
CM: 0000-0001-6871-7188
MA: 0000-0003-0087-4819
OS: 0000-0002-2613-0714

Corresponding authors: Glen G D'Souza and Astrid KM Stubbusch
Address: Eawag, Ueberlandstrasse 133, 8600 Duebendorf, Switzerland
Email: glengeralddsouza@gmail.com, astubbusch@icloud.com
Phone: +41-58-765-5495

Keywords: cooperative polysaccharide degradation, colony formation, cell dispersal, glycan, alginate, exoenzymes, alginate lyases, *Vibrio cyclitrophicus* ZF270

Abstract

Most of Earth's biomass is composed of polysaccharides. During biomass decomposition, polysaccharides are degraded by heterotrophic bacteria as a nutrient and energy source and are thereby partly remineralized into CO_2. As polysaccharides are heterogeneously distributed in nature, following the colonization and degradation of a polysaccharide hotspot the cells need to reach new polysaccharide hotspots. Even though these degradation-dispersal cycles are an integral part in the global carbon cycle, we know little about how cells alternate between degradation and motility, and which environmental factors trigger this behavioral switch. Here, we studied the growth of the marine bacterium *Vibrio cyclitrophicus* ZF270 on the abundant marine polysaccharide alginate. We used microfluidics-coupled time-lapse microscopy to analyze motility and growth of individual cells, and RNA sequencing to study associated changes in gene expression. Single cells grow at reduced rate on alginate until they form large groups that cooperatively break down the polymer. Exposing cell groups to digested alginate accelerates cell growth and changes the expression of genes involved in alginate degradation and catabolism, central metabolism, ribosomal biosynthesis, and transport. However, exposure to digested alginate also triggers cells to become motile and disperse from cell groups, proportionally increasing with the group size before the nutrient switch, accompanied by high expression of genes involved in flagellar assembly, chemotaxis, and quorum sensing. The motile cells chemotax toward alginate hotspots, likely enabling cells to find new polysaccharide hotspots. Overall, our findings reveal the cellular mechanisms underlying bacterial degradation-dispersal cycles that drive remineralization in natural environments.

Importance

Polysaccharides, also known as glycans, are the most abundant form of biomass on Earth and understanding how they are degraded by microorganisms is essential for our understanding of the global carbon cycle and the storage and release of CO_2 by natural systems. Although group formation is a common strategy used by bacterial cells to degrade ubiquitous polymeric growth substrates in nature, where nutrient hotspots are heterogeneously distributed, little is known about how cells prepare for dispersal from an exhausted nutrient source and re-initiate degradation of new nutrient patches. By

quantifying growth, motility and chemotaxis of individual cells and comparing gene expression changes when populations were exposed to either polysaccharides or their degradation products in the form of digested polysaccharides, we show that bacterial cells alter their behavior when they experience a shift from polymeric to digested polysaccharides: After cells form groups during growth on polymers, the exposure to degradation products made cells motile, enabling dispersal from sessile cell groups and - guided by chemotaxis - movement towards new polysaccharide hotspots. Our study sheds light on the cellular processes that drive bacterial growth and behavior during carbon remineralization, an important driver of CO_2 release from biomass in natural systems.

Introduction

Polysaccharides represent the largest fraction of biomass on Earth[1,2] and are constantly degraded and remineralized by microorganisms. Polysaccharides, also known as glycans, are long chains of monosaccharide units produced by cells for structural support (e.g., cellulose, chitin, and alginate) or energy storage (e.g., starch or glycogen)[1]. Heterotrophic microbes obtain nutrients and energy from the polysaccharide breakdown products. They often use exoenzymes, either secreted or anchored in the cell membrane[2,3], to cleave these large polymers into smaller units that can be taken up by cells. The formation of dense cell groups is observed during growth on polysaccharides by diverse bacteria, including the soil- and gut-dwelling *Bacillus subtilis*[3], the oligotrophic fresh-water *Caulobacter crescentus*[4], and several representatives of the copiotrophic[5,6] marine *Vibrio spp.*[7,8]. It has been suggested that "cooperative" growth[3], where dense cell groups reduce diffusional loss of valuable degradation products and secreted exoenzymes, represents a general principle in polysaccharide degradation[4,8]. Yet, how bacteria subsequently disperse from exhausted polysaccharide sources and navigate towards new polysaccharide hotspots remains poorly understood.

To study the cellular mechanisms that govern the switch between polysaccharide degradation and dispersal toward new polysaccharide hotspots, we worked with the ubiquitous marine Gammaproteobacterium *Vibrio cyclitrophicus* ZF270, a degrader of the prevalent marine polysaccharide alginate[6,9]. Alginate is a linear polysaccharide that is produced by brown algae as a cell

97 wall component, as well as by certain bacteria[10]. It can be cleaved into oligomers by endo-acting alginate
98 lyases or into monomers by exo-acting alginate lyases (alginate lyases reviewed here[11]), namely β-D-
99 mannuronic acid and α-L-guluronic acid[10]. *V. cyclitrophicus* ZF270 is found predominantly in the large-
100 particle fractions of coastal water[12], can attach and form biofilms on the surfaces of multiple
101 polysaccharides including alginate[13], and was shown to secrete alginate lyases during alginate
102 degradation[8]. In this study, we used microfluidics coupled to automated time-lapse imaging to quantify
103 the growth dynamics, group formation, and motility of *V. cyclitrophicus* ZF270 at the single-cell level
104 under constant supply of either polymeric alginate or alginate degradation product in the form of
105 digested alginate, as well as upon a transition from alginate to digested alginate. Furthermore, we used
106 RNA-sequencing to compare the gene expression of *V. cyclitrophicus* ZF270 grown on alginate and
107 digested alginate. We found striking responses to the form of alginate in growth rate, group formation,
108 motility and chemotaxis, as well as in the expression of corresponding genes. Overall, our work
109 provides insights into the metabolic and cellular regulation that allows cells to forage in heterogeneous
110 nutrient-scapes through degradation-dispersal cycles.
111
112 **Results**
113 **Extracellular break down of alginate delays population growth**
114 To probe the phenotypic and metabolic regulation of bacterial cells during the progressive degradation
115 of a polysaccharide source, we developed an experimental system consisting of the marine bacterium
116 *V. cyclitrophicus* ZF270 growing on alginate, a highly abundant polysaccharide in the ocean. To mimic
117 the local nutrient environment during the colonization of a new polysaccharide source, we used 0.1%
118 weight per volume (w/v) algae-derived alginate in its soluble form (in the following also simply referred
119 to as "alginate"). Since commercially available alginate breakdown products of specific sizes are limited
120 and expensive, with only one monomeric component available at a considerable cost, we simulate an
121 advanced stage of polysaccharide degradation by supplying cells with digested alginate (0.1% (w/v)).
122 This digested alginate is prepared by treating alginate with a readily available endo-acting alginate lyase
123 (see Materials and Methods). This mimics an environment where degradation products like monomers
124 and oligomers become abundant through the action of extracellular alginate lyases. The commercially

125 available alginate lyase has been shown to produce alginate oligomers of progressively smaller size
126 over extended digestion periods[14,15]. We used Liquid Chromatography-Mass Spectrometry (LC-MS) to
127 analyze the composition of the digested alginate, which had been subject to 48 hours of digestion. We
128 found that digested alginate contained more monosaccharides than untreated alginate, which contained
129 more alginate molecules of higher molecular weight (Fig. S1).
130
131 Using this system, we first set out to investigate the growth dynamics of *V. cyclitrophicus* ZF270 in
132 well-mixed batch cultures containing either alginate or digested alginate as a sole carbon source (Fig.
133 S2A). We found that similar yields were reached in the alginate and digested alginate cultures as
134 indicated by optical density (Fig. S2B and C) and confirmed by colony counts (Fig. S3), suggesting that
135 the same amount of alginate supports a similar yield irrespective of its degree of depolymerization.
136 However, the onset of growth on alginate was delayed by about 7.5 hours compared to growth on
137 digested alginate (Fig. S2D and E). This is consistent with previous observations that in well-mixed
138 environments the lag time of bacteria growing on alginate can be reduced by the external
139 supplementation of alginate lyases[8,14]. Together, these findings indicate that growth on polysaccharides
140 such as alginate in well-mixed cultures is initially limited by the extracellular breakdown of the
141 polysaccharide.
142
143 **Large cell groups form on alginate but not on digested alginate**
144 To better understand how cells react to the changing degree of depolymerization of a polysaccharide
145 source during degradation, we investigated the growth of *V. cyclitrophicus* ZF270 at the level of single
146 cells on alginate and digested alginate. For this purpose, we grew the cells in microfluidic growth
147 chambers, described in detail by Dal Co et al.[16], where cells were provided with a continuous flow of
148 culture media containing either alginate or digested alginate as carbon source. We found that over 24
149 hours dense groups of more than 1000 cells formed on alginate, filling the entire microfluidic chamber
150 (Fig. 1A). In contrast, cells supplied with digested alginate grew in smaller groups that never exceeded
151 100 cells per chamber (Fig. 1B and C). Reconstructed cell lineages revealed that the large cell groups
152 on alginate formed because cells often did not disperse after division and thereby formed dense cell

153 groups originating from a single cell lineage (Fig. 1A). The lower cell density on digested alginate could
154 be caused by slower growth or by more cells leaving the chambers. As the maximum growth rate both
155 in bulk and on single cell level is similar in alginate and digested alginate (Fig. S2E and F), it is most
156 likely that the lower cell density in digested alginate is caused by cell dispersal. These observations
157 suggest that cells can modulate their propensity to form groups depending on the state of polysaccharide
158 degradation in their local environment. Similar observations were made with a different model system
159 (*Caulobacter crescentus* growing on the polysaccharide xylan)[14], indicating that group formation on
160 polymeric nutrient sources may be a general mechanism of bacteria that degrade polysaccharides
161 extracellularly.
162

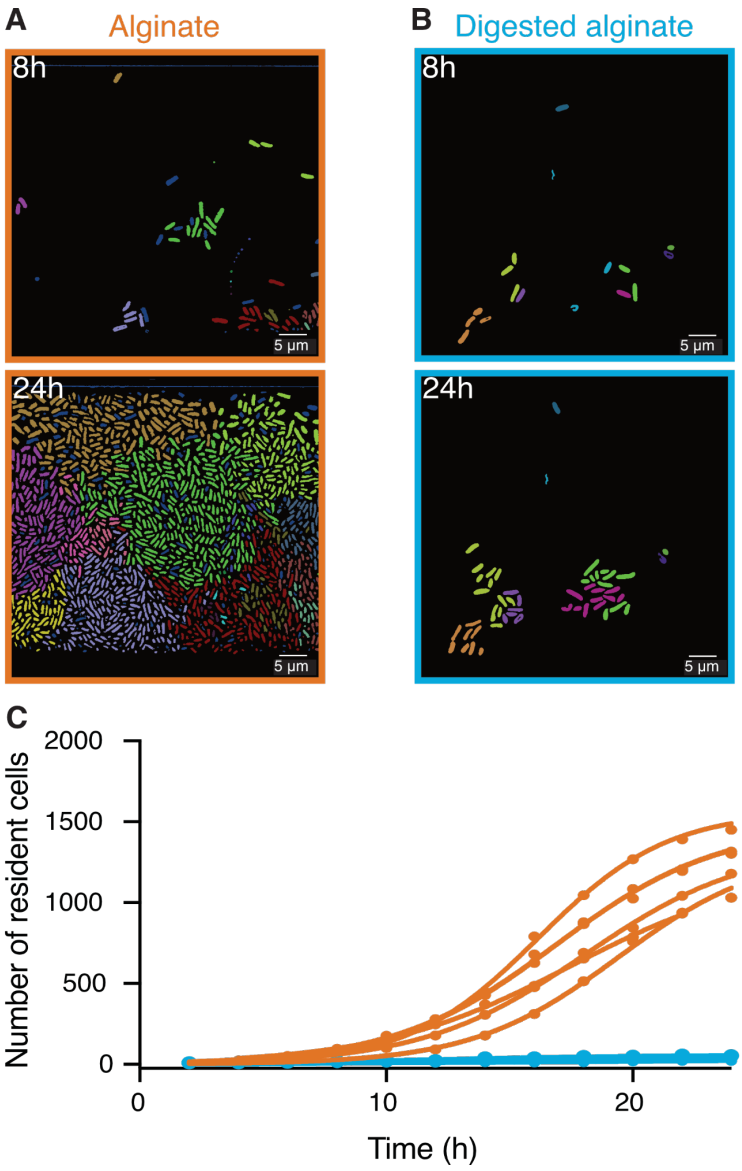

163

164 **Figure 1. Large cell groups form on alginate but not on digested alginate.** Representative images at different
165 time points of *V. cyclitrophicus* ZF270 cells growing in microfluidic chambers, described in detail by Dal Co et
166 al.[16], with (A) alginate medium or (B) digested alginate medium, both in their soluble form (not visible). Cells are
167 false-colored according to their lineage identities based on cell segmentation and tracking over 24 hours. Cells
168 without identified progenitors are colored in dark blue. See Supplemental Videos S1 (alginate) and S2 (digested
169 alginate) for time-lapse videos. (C) Cell numbers within microfluidic chambers supplied with alginate (orange)
170 are substantially higher than cell numbers within microfluidic chambers supplied with digested alginate (blue)
171 (Logistic growth regression for alginate: $R^2 = 0.99$, maximal number of cells = 1217-1564, k = 0.24-0.38 h^{-1}; for
172 digested alginate: $R^2 = 0.86$-0.97, maximal number of cells = 47-100, k = 0.07-0.4 h^{-1}). Circles indicate the number
173 of cells present at a given time point in each chamber ($n_{chambers} = 7$). Data for chambers with alginate originate
174 from D'Souza et al.[8]. Lines are fits of a logistic growth regression line for each condition.
175

176 **Transition from alginate to digested alginate triggers density-dependent dispersal of cells**

177 To investigate the transition from the large cell groups formed on alginate to the small groups formed
178 on digested alginate, we subjected *V. cyclitrophicus* ZF270 cells grown on alginate to a switch to
179 digested alginate (Fig. 2A). Following the limited cell motility on alginate, this switch led to a rapid
180 decrease in cell density within the growth chambers (Fig. 2B), presumably caused by cell dispersal. As
181 we previously reported for other *Vibrionaceae* isolates, the growth rate of the cells on alginate was
182 dependent on the local cell density: Initially the growth rate increased with cell density but then
183 decreased at high cell densities, indicating that cell groups can benefit from the sharing of breakdown
184 products generated by each other's exoenzymes, but also increasingly compete for nutrients[8]. This led
185 us to investigate whether cell in larger groups, potentially experiencing stronger nutrient competition,
186 might have a higher propensity to disperse after a switch to digested alginate than cells in smaller
187 groups. We indeed found an inverse relationship between the number of cells at the time of the nutrient
188 switch and the following change in cell number, meaning that cells in chambers with many cells were
189 more likely to disperse than cells in chambers with less cells (Fig. 2C). Thus, during the transition from
190 polysaccharides to degradation products, we found that the dispersal rate of cells depends on the size of
191 the cell groups, likely through increased motility of cells in large groups.
192

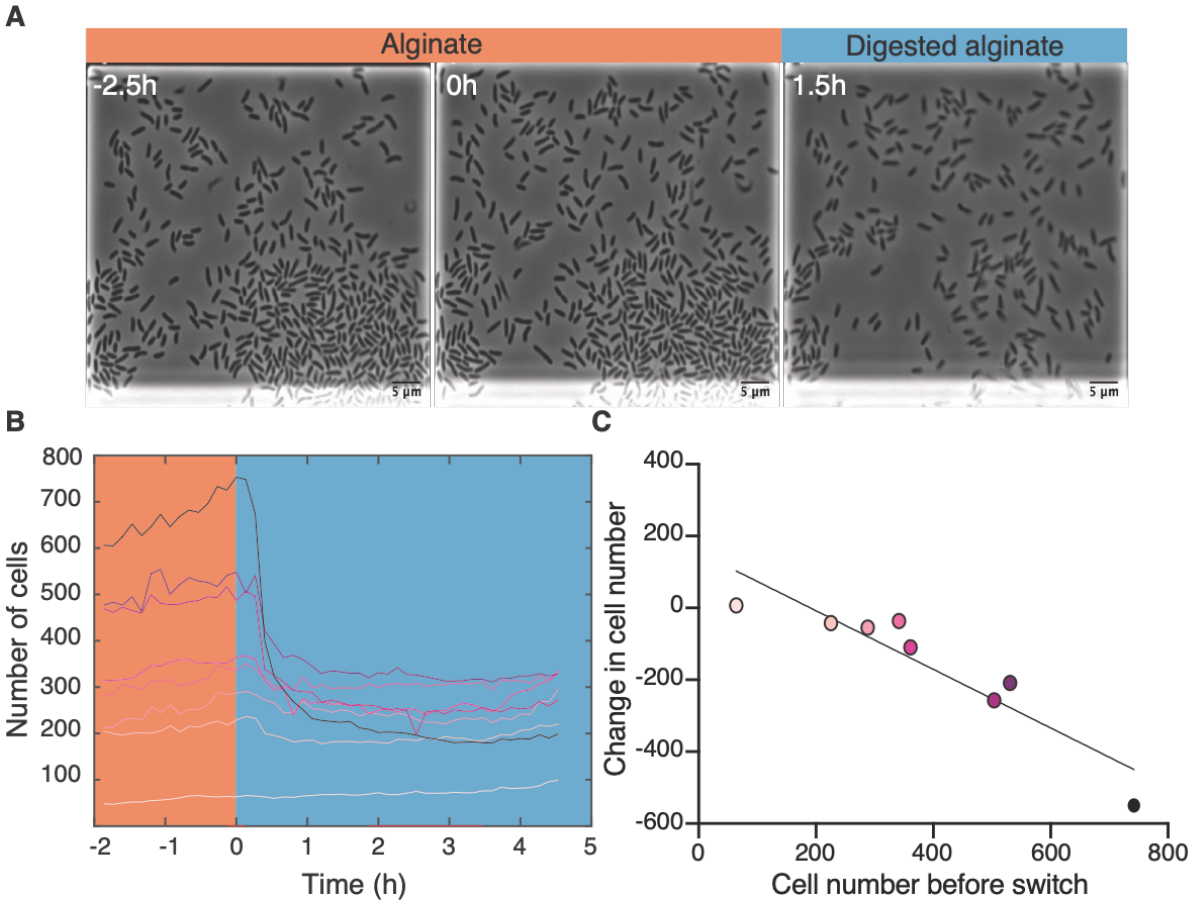

Figure 2. Transition from alginate to digested alginate triggers density-dependent dispersal of cells. (A) Representative time-lapse images of *V. cyclitrophicus* ZF270 cells (phase contrast microscopy) in microfluidic growth chambers that were initially exposed to alginate and then switched to digested alginate. (B) Number of cells in different chambers over time, each chamber indicated by a unique color (n = 8). The carbon source is indicated by the colored background (orange: alginate; blue: digested alginate). See Supplemental Video 3 for a time-lapse video. (C) Negative relationship between the difference in number of cells within the microfluidic growth chambers before and after the nutrient switch. Each circle represents one growth chamber with colors corresponding to (B), and the line depicts a linear regression fit (R^2 = 0.85, slope = -0.81, p-value < 0.001).

Cells growing on digested alginate are more motile and chemotax towards new polysaccharide sources

To investigate whether increased cell motility of *V. cyclitrophicus* ZF270 underlies the dispersal of cells observed after a shift to digested alginate, as also previously observed for *C. crescentus* cells on the monosaccharide xylose[4,14], we quantified the motility of single cells supplied with either alginate or digested alginate. We found that the single-cell swimming speed as well as the swimming distance were

209 significantly larger for cells supplied with digested alginate compared to cells supplied with alginate,
210 and that a larger fraction of cells was motile (Fig. 3). This confirmed increased motility as a cellular
211 response to the exposure to degradation products in the form of digested alginate.
212
213 To understand if the motile cells are directed by chemotaxis, we measured the chemotactic strength
214 towards alginate and digested alginate using the In Situ Chemotaxis Assay (ISCA)[17,18]. We found *V.*
215 *cyclitrophicus* ZF270 to significantly chemotax toward alginate (chemotactic index $I_c > 1$) but not
216 toward digested alginate (Fig. 3F). This suggested that the increase in motility is accompanied by
217 chemotaxis toward alginate. Overall, these findings suggest that once the breakdown of a
218 polysaccharide source makes breakdown products available in the local environment, a fraction of cells
219 becomes motile and disperses. These motile cells are guided by chemotaxis towards new polysaccharide
220 sources, allowing them to start a new degradation-dispersal cycle.
221
222 **Altered gene expression in central carbon metabolism, enzyme production, secretion and**
223 **transporters, motility, and quorum sensing underlies the late-stage alginate degradation and cell**
224 **dispersal**
225 Next, we sought to elucidate the molecular mechanisms underlying the observed phenomenological
226 disparities between cells cultivated on alginate and digested alginate. Due to the challenge of generating
227 knock-out mutants in natural isolates, we used transcriptomics to investigate the differentially expressed
228 genes of *V. cyclitrophicus* ZF270 under these respective conditions. To obtain a high-quality reference
229 genome of *V. cyclitrophicus* ZF270, we sequenced and assembled a new reference genome using
230 combined short and long read sequencing (BioProject PRJNA991487). We then grew cultures on either
231 alginate or digested alginate until mid-exponential phase. To understand which cellular functions were
232 affected by the expression changes, we first performed differential gene expression analysis using the
233 software DESeq2. Here, genes exhibiting a log2 fold expression change greater than 0.5 or smaller than
234 -0.5 between the two conditions, with a Benjamini-Hochberg(BH)-adjusted *p*-value below 0.01, were
235 considered to be differentially expressed (Table S1). Next, we investigated which KEGG categories

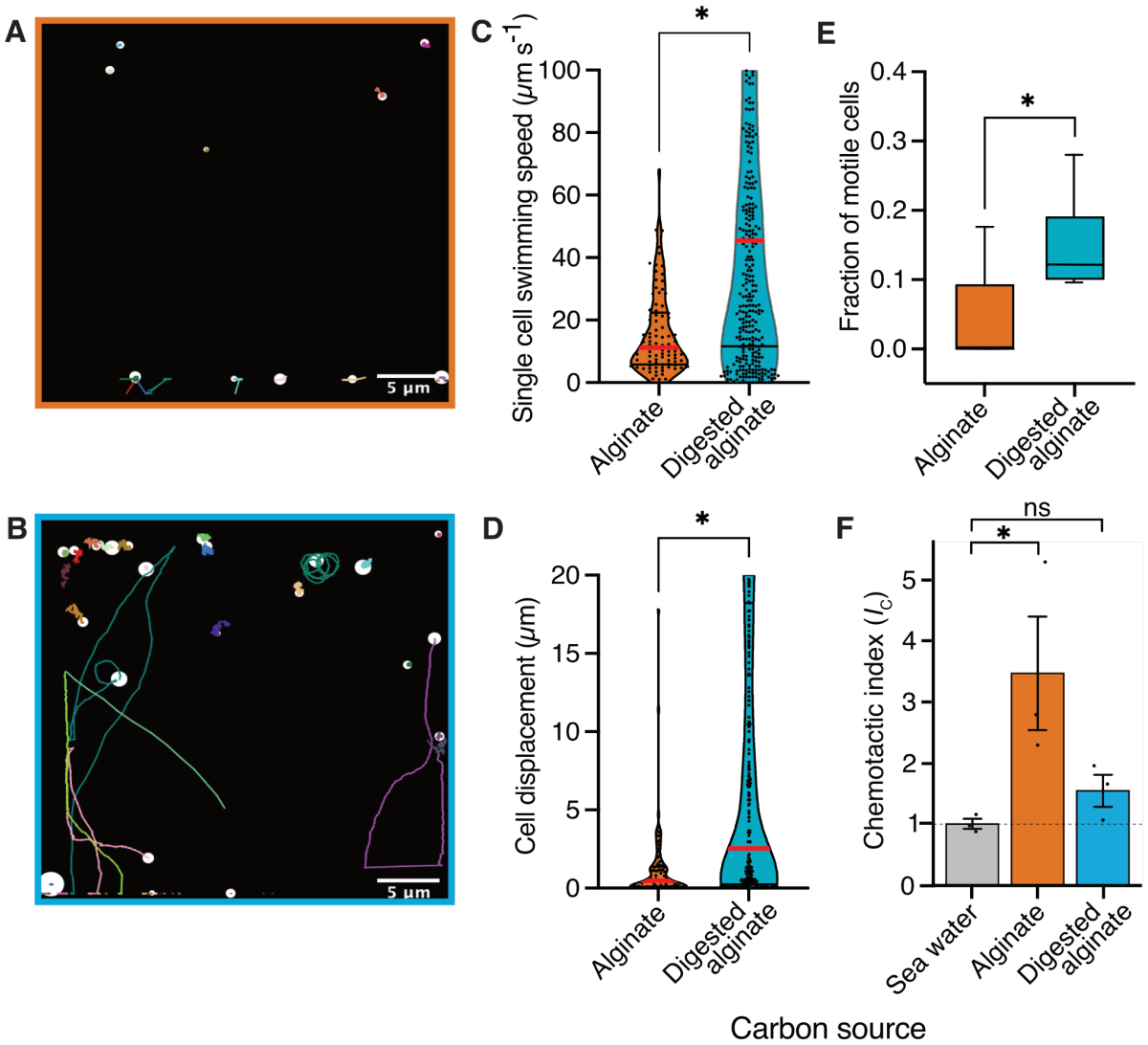

Figure 3. Cells are more motile on digested alginate than alginate and show chemotaxis towards alginate. (A and B) Spatial trajectories of cells supplied with (A) alginate or (B) digested alginate in representative microfluidic growth chambers are shown. White circles mark the starting point of each trajectory and colored lines mark the individual trajectories. (C) Distributions of the mean single-cell swimming speeds (Nested t-test, p-value < 0.0007, t = 4.803, df = 10, n_{cells} = 86 vs 375 in $n_{chambers}$ = 5) are shown. (D) Distributions of cell displacement over the course of a trajectory (Nested t-test test, p-value < 0.0131, t = 4.39, df = 10, n_{cells} = 86 vs 375, and $n_{chambers}$ = 5) are shown. In (C) and (D) the red horizontal lines indicate the mean while black lines depict the 25th and 75th quartiles of the distribution. (E) The mean fraction of motile cells in each chamber, where motile cells are defined as cells with displacement greater than 1 µm (Mann-Whitney test on the means of five growth chambers, p-value = 0.034). In C, D, and E, each chamber was considered as an independent replicate. (F) Chemotactic index (I_C) quantified by In Situ Chemotaxis Assay (ISCA) (Tukey multiple comparisons of means,

248 95% family-wise confidence levels as error bars, *p*-value < 0.05, n = 3). Asterisks indicate statistically significant
249 differences. See Supplemental Videos S4 and S5 for time-lapse videos of swimming cells.
250
251 were enriched in either genes with increased or decreased expression via Gene Set Enrichment Analysis
252 (GSEA)[19] (Table S2) and found nine categories significantly enriched in genes with increased gene
253 expression on digested alginate, and three categories significantly enriched in genes with decreased
254 gene expression (Fig. 4A).
255
256 Cells growing on digested alginate showed expression changes in parts of the central metabolism and
257 translation, compared to cells growing on alginate. Specifically, two pathways of the central metabolism
258 were significantly enriched in genes with lower expression on digested alginate ("Valine, leucine and
259 isoleucine biosynthesis" and "Propanoate metabolism" with a negative normalized enrichment score
260 (NES), Fig. 4A, S4A and B, Table S3 and S4). We also found the gene set that encodes ribosomal
261 proteins significantly enriched with genes highly expressed on digested alginate (positive NES, Fig. 4A
262 and S4C, Table S5). This implies that cells invest proportionally more of their transcriptome into the
263 production of new proteins, a sign of faster growth[20,21]. Both observations likely relate to the different
264 growth dynamics of *V. cyclitrophicus* ZF270 on digested alginate compared to alginate.
265
266 The expression of transporters and secretion systems was generally increased in cells growing on
267 digested alginate, compared to cells growing on alginate. This includes genes with a function in
268 "Bacterial secretion systems", namely secretion systems I to VI, which mediate protein export through
269 the inner and outer membranes of Gram-negative bacteria (Fig. 4A and S4D, Table S6). Notably, eleven
270 of the thirteen General Secretion Pathway (GSP) genes (part of the type II secretion system) showed
271 1.1 to 3.4-fold increased expression levels on digested alginate (*p*-values < 0.01, Fig. 4A, Table S8).
272 The GSP is known to facilitate secretion of various extracellular enzymes like chitinases, proteases, and
273 lipases[22,23], therefore, the positive enrichment on digested alginate may be linked to the export of
274 extracellular alginate lyases. The KEGG BRITE category "Secretion system" was also enriched on
275 digested alginate (Fig. 4A and S4D, Table S7). It contains additional genes involved in protein export,

276 of which especially genes of type IV pilus assembly, conjugal transfer pilus assembly, and MSHA pilus
277 biogenesis were highly expressed on digested alginate, implicating them as interesting subjects to
278 further research in their role in protein secretion and cell attachment and detachment during
279 degradation-dispersal cycles of polysaccharide-degrading bacteria. Also, the gene set of transporters
280 and in particular ABC transporters were positively enriched (Fig. 4A, Table S10 and S11). The latter
281 showed enrichment especially in genes related to saccharide, iron, zinc, and phosphate transport (Fig.
282 S4E), which suggests that cells growing on digested alginate invest proportionally more of their
283 transcriptome into uptake of not only saccharides but also essential nutrients like iron, zinc, and
284 phosphate, which may become growth-limiting when degradation products are abundantly available.
285
286 Both motility and quorum sensing genes increased in expression in cells growing on digested alginate.
287 The positive enrichment of the gene set containing bacterial motility proteins matched the increase in
288 motile cells that we observed in Figure 3E (Fig. 4A, Table S12). The set of quorum sensing genes was
289 also positively enriched in cells growing on digested alginate (Fig. 4A and S4F, Table S13). Quorum
290 sensing is known to control biofilm formation in *Vibrio cholerae*[24,25] and may orchestrate the density-
291 dependent dispersal in the presence of degradation products, though the particular signaling cues remain
292 to be uncovered. The strong cellular response to the degree of alginate depolymerization was also
293 emphasized by the finding that transcription factor genes were enriched among genes with decreased
294 expression on digested alginate (Fig.4, Table S14). The set of genes associated to KEGG's beta-lactam
295 resistance category was enriched in genes with increased expression on digested alginate. However,
296 most genes in this gene set are also associated to the KEGG pathways "Transporters", "Quorum
297 sensing", "Chromosome and associated genes", and "Peptidoglycan biosynthesis" and thus the
298 enrichment likely reflects expression changes in these categories and may relate to the difference in
299 growth dynamics (Fig. 4A and S4G, Table S15). Overall, the observed gene expression changes provide
300 insights into the molecular mechanisms underlying the substantial adaptations of *V. cyclitrophicus*
301 ZF270 cells to the polymeric and digested form of alginate.
302

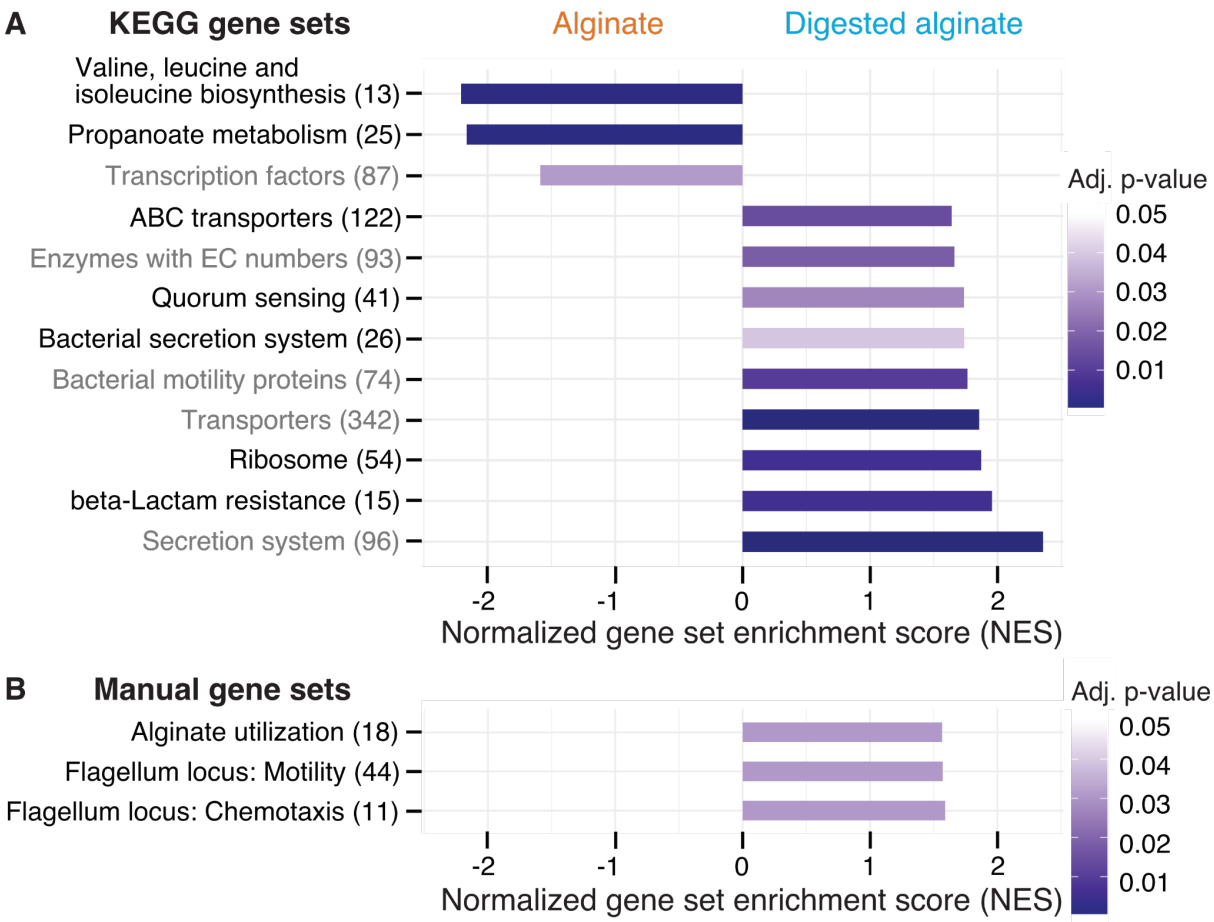

Figure 4. Twelve functional gene sets are enriched in genes with increased or decreased expression in cells grown on digested alginate. Gene set enrichment analysis (GSEA) with (A) all KEGG pathways and KEGG BRITE categories as gene sets or with (B) a custom alginate utilization, flagellar assembly, and flagellum-driven chemotaxis gene set was performed comparing the gene counts of the transcriptome of *V. cyclitrophicus* ZF270 cultures grown on digested alginate and alginate (six replicates each). Gene sets with a positive enrichment score were enriched with genes with higher expression in cells grown on digested alginate relative to cells grown on alginate (BH-adjusted p-value < 0.05), whereas gene sets with negative enrichment scores were significantly enriched with genes with decreased expression on digested alginate. The number in brackets indicates the number of genes with unique K number per gene set (A) and the number of genes per gene set (B) within the *V. cyclitrophicus* ZF270 genome.

Growth on digested alginate is associated with increased expression of alginate catabolism, flagellar motility and chemotaxis genes

For a more fine-grained understanding of the impact of the form of alginate on the alginate catabolism, we investigated specifically the expression of genes involved in alginate degradation, uptake, and

319 catabolism. In the closed genome of *V. cyclitrophicus* ZF270, we identified genes that encode CAZymes
320 responsible for alginate degradation, namely alginate lyase genes from the PL6, PL7, PL15, and PL17
321 family. We identified homologs of alginate transporters (porin *kdgM*, symporter *toaA*, *toaB*, and *toaC*)
322 and metabolic enzymes that shunt into the Entner-Doudoroff pathway (DEHU reductase genes *dehR*,
323 *kdgK*, and *eda*), based on the known genes in the alginate degradation pathway of *Vibrionaceae*[26,27].
324 We found that the expression of most of these genes increased significantly on digested alginate relative
325 to alginate (Fig. 4B, Fig. 5A, S8A, Table S16). Surprisingly, also the expression of most alginate lyase
326 genes increased on digested alginate, especially the expression of secreted alginate lyase genes. This
327 indicates the production of "public" exoenzymes despite the abundance of monomeric and oligomeric
328 degradation products in the digested alginate medium.
329
330 The increased motility of cells observed upon exposure to digested alginate (Fig. 3, Fig. 4A) led us to
331 evaluate the expression of motility- and chemotaxis-associated genes across digested alginate and
332 alginate treatments. As flagella are the main mode of motility in the genus *Vibrio*[28,29], we focused on
333 the expression of flagella-related genes. In the genome of *V. cyclitrophicus* ZF270 we found a gene
334 cluster that encodes most genes involved in flagellar assembly and that was flanked by chemotaxis
335 genes (hereon called flagellar locus, Fig. S8B, and Table S17). Overall, 21/34 flagellar locus genes were
336 differentially expressed (log2 fold change > 0.5, BH-adjusted *p*-value < 0.01) and the majority (90%)
337 of these differentially expressed genes showed increased expression on digested alginate (Fig. 4B). The
338 flagellar genes *flgA*, *fliC*, and *fliH* and the chemotaxis gene *cheW* showed the strongest overexpression
339 (5.4, 3.8, 2.0, and 2.6-fold, respectively). The expression of flagellar biosynthesis genes in *Vibrionacaea*
340 occurs by a cascade of gene expression of four classes of genes (Class I - IV)[30]. We found the expression
341 of the master regulator of the flagellar biosynthesis regulon, the Class I gene *flrA*, to be 1.6-fold
342 increased on digested alginate (BH-adj. *p*-value 3e-19)[31]. The Class II regulatory genes *flrBC*,
343 controlling Class III genes, and *fliA*, controlling Class IV genes, showed 1.5-fold and 1.3-fold increased
344 expression on digested alginate (BH-adj. *p*-value 1e-12 for *flrB*, 2e-39 for *flrC*, 6e-15 for *fliA*) (Fig.
345 5B)[29,32]. These findings suggest that the increased phenotypic motility observed on digested alginate
346 (Fig. 3) is related to the upregulation of flagellar biosynthesis genes. Additionally, the expression of the

flagellum filament, encoded by *fliC* genes of the flagellar locus, was partially increased: *flaD* and *flaC* expression were increased by 3.8 and 1.6-fold, whereas the *flaA* gene was not significantly differentially expressed (BH-adj. *p*-value 7e-37, 2e-19, and 1e-02, respectively) (Fig. 5B, Table S6). This suggests that cells grown on digested alginate have a *flaD*-rich filament composition, which has been shown to alter the swimming and adhesion characteristics of bacterial cells[33,34]. Lastly, we found that most genes involved in chemotaxis and located in the flagellar locus are highly expressed in cells grown on digested alginate (Fig. 5C, Fig. 4B) and likely drive the chemotactic activity of *V. cyclitrophicus* ZF270 during dispersal. Overall, our findings elucidate that cellular responses upon exposure to degradation products manifest in increased expression of genes involved in extracellular alginate breakdown and alginate catabolism as well as flagellar assembly and chemotaxis.

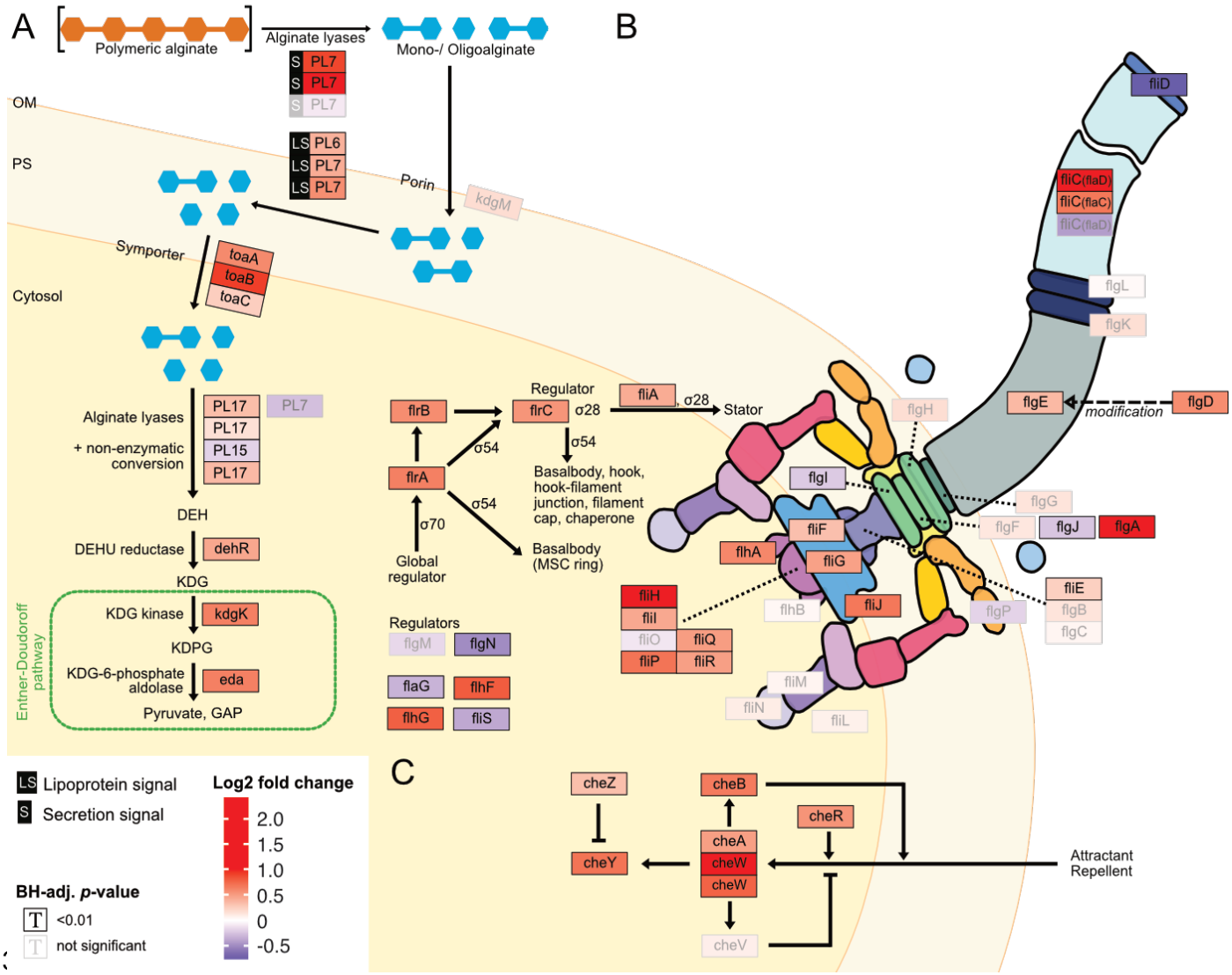

358 **Figure 5. Digested alginate increases expression of genes involved in alginate degradation, uptake and**
359 **catabolism, as well as flagellar assembly and chemotaxis.** Genome-wide differential expression analysis where
360 the log2 fold changes of gene expression on digested alginate compared to alginate is shown for (A) alginate
361 lyases (*PL6, PL7, PL15, PL17*), transporters (porin *kdgM*, symporter *toaB*, symporter *toaC*), and metabolic
362 enzymes shunting into the Entner-Doudoroff pathway (DEHU reductase *DehR*, *kdgK*, *eda*), (B) genes of the
363 flagellar locus associated with flagellar assembly and (C) adjacent chemotaxis genes. Genes displayed in (B) and
364 (C) are part of the KEGG pathways "Bacterial motility proteins" and "Bacterial chemotaxis". Differential
365 expression analysis was performed to compute the Benjamini-Hochberg-adjusted Wald test *p*-value ("BH-adj. *p*-
366 value", text color and box outline color) and log2 fold change (box fill color) for each gene (box). For better
367 visibility, genes that exhibited a log2 fold gene expression change greater than 1 (i.e., doubling of expression) or
368 less than -1 (i.e., halving of expression) are designated maximum intensity of red or blue, respectively. Genes with
369 BH-adj. *p*-value smaller than 0.01 were considered significantly differentially expressed. In (A), the location of
370 the gene products was based on Figure 1 of Wargacki et al.[26] with the exception of the alginate lyases (*PL6*, *PL7*,
371 *PL15*, *PL17*) which were placed based on their signal peptides (S: extracellular, LS: membrane-embedded, none:
372 cytosolic). In (B) and (C) the gene location and depiction were based on the KEGG pathway "Flagellar assembly"
373 (map02040), "Bacterial chemotaxis" (map02030), and Figure 3 of Rajagopala et al.[35]. Genes without known
374 cellular location were omitted here but displayed in the genomic architecture in Fig. S5. Arrow: activation; dashed
375 arrow: modification; "flat" arrow: inhibition; OM: outer membrane; PM: periplasm; IM: inner membrane; PL:
376 polysaccharide lyase family; *kdgM*: oligogalacturonate-specific outer membrane porin; *toaABC*: oligoalginate
377 symporter; DEH: 4-deoxy-L-erythro-5-hexoseulose uronic acid; *dehR*: DEH reductase; KDG: 2-keto-3-deoxy-
378 gluconate; *kdgK*: KDG kinase; KDPG: 2-keto-3-deoxy-6-phosphogluconate; *eda*: KDG-6-phosphate aldolase;
379 GAP: glyceraldehyde 3-phosphate; ED: Entner-Doudoroff; ns: not significant, i.e. BH-adj. *p*-value > 0.01.
380

381 **Discussion**

382 On Earth organic carbon is mostly present in the form of polysaccharides[1,2], which are often in a
383 particulate state and form a heterogeneous resource landscape. Over the last years, the study of
384 extracellular bacterial degradation of polysaccharides has revealed that bacterial growth on
385 polysaccharides increases with increased cell density, enabling cells to benefit from the exoenzymes
386 and extracellular degradation products of surrounding cells otherwise lost to diffusion ("cooperative

387 growth")[36–38]. However, cells have been observed not only to aggregate on polysaccharide sources, but
388 also to leave them before the source is depleted[13,38]. This has thus far been interpreted with optimal
389 foraging theory, which weighs the diminishing returns of harvesting resources from a nutrient hotspot
390 against the predation and opportunity costs which ensue[39,40], but the cellular mechanisms that drive the
391 cell dispersal remain unclear.
392
393 Our work links these observations and connects them to the cellular mechanisms that underlie the
394 degradation-dispersal cycles of bacterial degraders, which we see as basal drivers of the biogeochemical
395 processing of polysaccharides in heterogeneous nutrient-scapes. When bacteria encounter a new source
396 of biomass, their local environment likely contains few mono- or oligosaccharides but is rich in
397 polysaccharides which usually require extracellular breakdown (Fig. 6, "Finding a new nutrient
398 source"). General concepts of how bacteria recognize the presence of large biopolymers remain elusive,
399 but it was proposed that "sentry" enzymes are constitutively expressed at a basal level to cleave mono-
400 or oligosaccharides from polysaccharides, which cells can take up and which prime their metabolism
401 for the degradation of the respective polysaccharide[41,42]. It is not known yet how widespread the concept
402 of sentry enzymes may be, but the observation of a constitutively expressed PL7 and PL15 family
403 alginate lyase gene in *Z. galactanivorans*[41] is mirrored in our work by the constant expression of an
404 extracellular PL7 family alginate lyase gene, which may act as sentry enzyme that helps to initiate
405 alginate degradation when cells encounter alginate.
406
407 It has been previously found that cells grow slowly until a critical cell density for efficient cooperative
408 polymer breakdown is reached[36], observed here as the formation of large cell groups. In this stage, cells
409 start to benefit from the diffusing degradation products and exoenzymes of cells in their local
410 environment and reach their maximal growth rate (Fig. 6, "Early-stage polysaccharide breakdown").
411 We found that cells grown on degradation products reached their maximal growth earlier and showed
412 increased expression of ribosomal biosynthesis, enzyme secretion, especially of secreted alginate
413 lyases, transporters, quorum sensing and expression changes in the central carbon metabolism. The
414 secretion of secreted alginate lyases might seem surprising and wasteful in a monomer-rich

415 environment. We speculate that enhanced enzyme secretion supports the continued growth of detached
416 bacteria's offspring that remain on the particle, as observed in the case of *V. splendus* 1AO1 during
417 chitin particle degradation[43]. Another reason may be that cells primarily rely on intracellular
418 monosaccharide levels to trigger the upregulation of genes associated with polysaccharide degradation
419 and catabolism, as seen in *E. coli* across various carbon sources[44,45], unable to modulate the expression
420 of degrading enzymes based on the extracellular presence of monomers.
421
422 We show that cells respond to the exposure to degradation products with dispersal from dense cell
423 groups by means of increased flagellum-driven swimming (Fig. 6, "Late-stage polysaccharide
424 breakdown"), decreasing their local cell number. This finding matches with previous observations of
425 cells leaving biopolymer particles before they are depleted[13,38]. A plausible explanation for this density-
426 dependent dispersal is that cells in larger groups compete with each other for nutrients and space, while
427 not profiting from cooperative degradation anymore due to the abundance of degradation products.
428 Motility has also been shown to increase the encounter rate of cells with sources of nutrients[46,47],
429 suggesting motility as a strategy that allows cells to escape from the ensuing competition. Previous
430 work in *Caulobacter crescentus* demonstrated that a flagellum knock-out mutant formed larger cell
431 groups, resulting in reduced growth rates due to intercellular competition[4,14]. While it would be
432 interesting to study non-motile mutants of *V. cyclitrophicus* ZF270, the non-tractability of natural
433 isolates makes direct tests of molecular mechanisms difficult. Additionally, subjecting cells separately
434 to the two monomeric units of alginate or oligomers of defined size could improve our understanding
435 of the specific molecules that trigger motility, but this was experimentally not feasible. We also found
436 that the presence of degradation products increased the expression of chemotaxis genes and detected
437 that cells chemotaxis toward polymeric alginate, but not digested alginate, analogous to previous
438 findings on chitin[46–48]. Even though this may first seem counterintuitive, it makes sense in the light of
439 the dispersal process: chemotaxis towards degradation products would prevent cells from leaving a
440 nutrient source, whereas chemotaxis towards polymers may increase encounters with a fresh nutrient
441 source[49] (Fig. 6, "Finding a new nutrient source"), on which cells can re-initiate degradation. This

442 strategy allows cells to alternate between degradation and dispersal to acquire carbon and energy in a
443 heterogeneous world with nutrient hotspots[50–53].
444

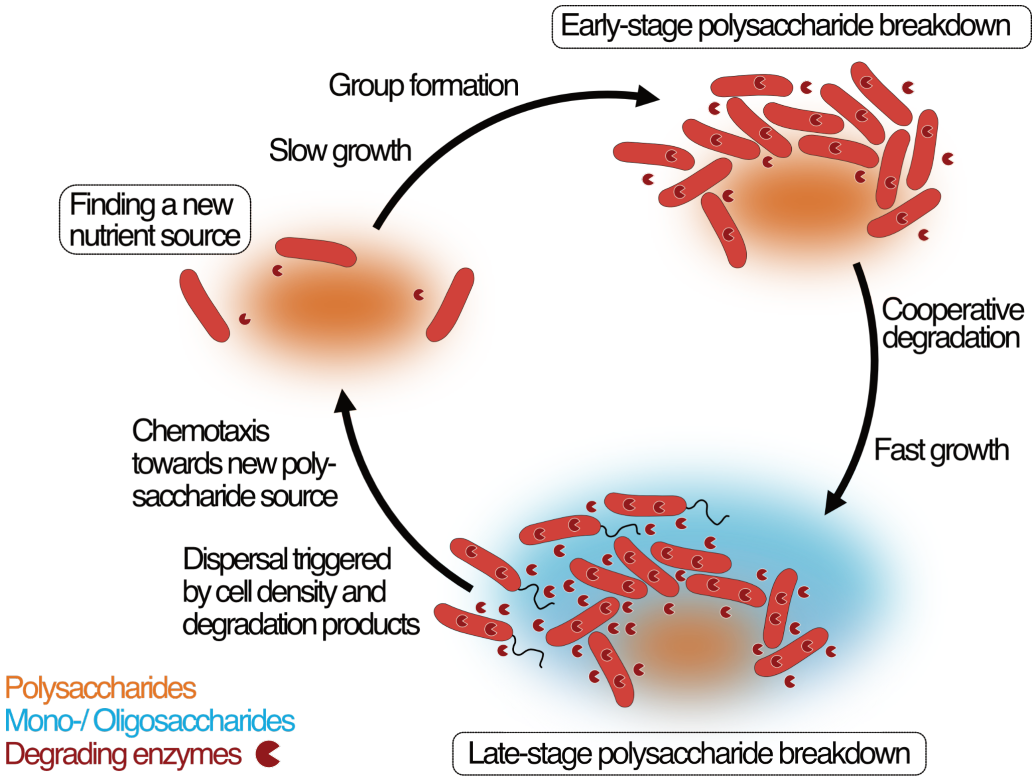

445
446 **Figure 6. Bacterial growth and regulation on patches of polysaccharides.** Based on our findings we propose
447 a conceptual model where degradation of polysaccharides proceeds after the encounter of a polymer source by
448 bacterial cells that have a basal exoenzyme production of "sentry" enzymes ("Encounter of a new carbon source").
449 This phase is succeeded by group formation, which enables cells to benefit from exoenzymes of neighboring cells
450 and diffusing degradation products ("Early-stage polysaccharide breakdown"). The following phase includes
451 cooperative extracellular degradation of the polysaccharide source, further increasing the concentration of
452 available degradation products. These degradation products trigger the overexpression of alginate degrading,
453 importing, and catabolizing enzymes, ensuring swift polysaccharide degradation ("Late-stage polysaccharide
454 breakdown"). The increased pool of breakdown products also cues flagellar swimming and chemotaxis in a
455 subpopulation of cells towards new polysaccharide sources, thus restarting the cycle of degradation of polymeric
456 carbohydrates by heterotrophic bacteria. Cells and molecules are not drawn to scale. Dark red pie symbols:
457 intracellular and extracellular polysaccharide-degrading enzymes; orange shading: a polymeric carbon source;
458 blue shading: monomeric or oligomeric degradation products.

459 **Conclusion**

460 The heterogeneous landscape of polysaccharide hotspots in natural systems requires bacteria to
461 effectively break down polymeric carbohydrates as well as readily ensure dispersal to new nutrient
462 hotspots. Our findings show that the degree of depolymerization of the polysaccharide influences this
463 decision, altering the growth dynamics, metabolic activity, and motility of cells. Our study also
464 contextualizes the surprising finding that foraging bacteria majorly leave polysaccharide particles
465 before the last third of the particle is consumed[38]. Dispersal from a partially degraded carbon source
466 may serve several purposes: (i) escaping competition that ensues within large cell groups, (ii) ensuring
467 the spread of a part of the clonal population to new environments as bet hedging strategy[40,54], here
468 guided by chemotaxis towards new nutrient hotspots, (iii) preventing whole populations degrading a
469 sinking marine particle or a deposited sediment particle to be buried in depth where nutrient hotspots
470 become sparse[38,55], and/or (iv) increase the genetic variation in bacterial populations[40]. However,
471 dispersal may also occur when a nutrient source offers a surplus of carbon while other essential nutrients
472 become limiting, as the increased expression of iron, zinc, and phosphate transporters in cells grown on
473 digested alginate suggested. These findings emphasize that metabolic molecules can also act as triggers
474 of dispersal, expanding upon the current perspective of dispersal in biofilms as a reaction to dispersal
475 cues like NO, signalling molecules, nutrient starvation, and oxygen starvation[56]. The study of bacterial
476 motility on increasingly complex biomass particles will reveal the role of the nutrient composition of
477 the present nutrient hotspot on the bacterial decision-making. Overall, these new insights into the
478 cellular mechanisms and regulation that drive degradation-dispersal cycles contribute to our
479 understanding of the microbially driven remineralization of biomass, and factors that modulate this
480 process. The open questions of how bacteria sense polysaccharides in their environment, which cell
481 signaling pathways integrate the presence of degradation products in the cellular decision-making of
482 degradation and dispersal, and to what extent cell populations coordinate this decision, present an
483 exciting avenue of further research.

484

485

486

487 **Materials and Methods**

488 *Bacterial strains, media and growth assays*

489 *Vibrio cyclitrophicus* ZF270 (available through Culture Collection Of Switzerland; Accession number:
490 2043) cells were cultured in Marine Broth (DIFCO) and grown for 18 hours at 25 °C. Cells from these
491 cultures were used for growth experiments in Tibbles Rawling (TR) salts minimal medium[57,58]
492 containing either 0.1% (weight/volume) algae-derived alginate (referred to as "alginate") (Sigma
493 Aldrich, CAS-number 9005-38-3) or 0.1% (weight/volume) digested alginate. The digested alginate
494 was produced by enzymatically digesting 2% alginate with 1 unit ml^{-1} of alginate lyase (Sigma Aldrich,
495 CAS-number 9024-15-1) at 37 °C for 48 hours. Carbon sources were prepared in nanopure water and
496 filter sterilized using 0.40 µm Surfactant-Free Cellulose Acetate filters (Corning, USA). Well-mixed
497 batch experiments in alginate or digested alginate medium were performed in 96-well plates (Greiner
498 Bio) and growth dynamics were measured using a microwell plate reader (Biotek, USA). Assays were
499 initiated as described previously[59]. Briefly, 1 ml from a culture grown for 18 h on Marine broth was
500 centrifuged at 5000 g in 1.5 ml microfuge tubes for 5 minutes. The supernatant was discarded and the
501 cell pellet was subjected to two rounds of washing with the basal TR salts medium. The cell-pellet was
502 then resuspended in 1 ml of TR salts medium and 5 µl of this suspension inoculated into 195 µl TR
503 medium with either carbon source (~10^5 colony forming units (CFUs ml^{-1}) in a 96-well plate (Greiner
504 Bio). The optical density (600 nm) was then measured every 15 minutes for 40 hours. All measurements
505 had six biological replicates.

506

507 *Alginate oligosaccharide measurements*

508 Oligosaccharide measurements were performed using liquid chromatography time of flight mass
509 spectrometry (LC-QTOF-MS). Samples were prepared by diluting 1:20 in milliQ water and 5 µL of
510 sample was injected per measurement. Chromatographic separation was performed using an Agilent
511 1290 stack, using an Agilent HILIC-Z column (2.7 µm particles, 2.1 x 50 mm). Mobile phase A
512 contained 10% acetonitrile (Fisher Scientific) and 0.1% medronic acid (Agilent), and Mobile phase B
513 contained 90% acetonitrile and 0.1% medronic acid. The separation was performed as follows: Mobile
514 phase B 100% for 1 minute, gradient to 30% phase B over 3 minutes, 30% phase B for 30 seconds, and

515 equilibration of 100% phase B for 5 minutes. The flow rate was 400 μL min^{-1} at 30 °C. Samples were
516 measured using an Agilent 6520 mass spectrometer in negative mode, in 4 GHz high-resolution mode.
517 Data analysis was performed in Agilent Quantitative Analysis software.
518
519 *Microfluidics and time-lapse microscopy*
520 Microfluidic experiments and microscopy were performed as described previously[14,16,60]. Cells were
521 imaged within chambers of a PDMS (Sylgard-Dow) microfluidic chip that ranged in size from 60-120
522 × 60 × 0.56 μm ($l \times b \times h$). Within these chambers, cells can attach to the glass surface and experience
523 the medium that diffuses through lateral flow channels. Imaging was performed using IX83 inverted
524 microscope systems (Olympus, Japan) with automated stage controller (Marzhauser Wetzlar,
525 Germany), shutter, and laser-based autofocus system (Olympus ZDC 2). Chambers were imaged in
526 parallel on the same PDMS chip, and phase-contrast images of each position were taken every 8 or 10
527 minutes. The microscopy unit and PDMS chip were maintained at 25 °C using a cellVivo microscope
528 incubation system (Pecon GmbH).
529
530 *Motility assays*
531 Cells were grown for 10 hours in Marine Broth (DIFCO) after which 10 μl of culture was used to
532 inoculate culture tubes (Greiner) containing 5 ml of TR medium with either 0.1% alginate or 0.1%
533 digested alginate. After 6 hours of growth at 25 °C, 2 μl of cell suspension was inoculated into
534 microfluidic growth chambers. Cells within six replicate chambers were then imaged with the phase-
535 contrast channel at a high frame rate (125 Hz, i.e., frames s^{-1}) using the same microscopy setup described
536 above.
537
538 *Chemotaxis assays*
539 To assess whether polymeric alginate and digested alginate attract *Vibrio cyclitrophicus* ZF270, we
540 used the *In Situ* Chemotaxis Assay[17,18] (ISCA), a microfluidic device consisting of a 5 × 5 array of
541 microwells that can be individually loaded with solutions of different chemicals (110 μl each). Once
542 the ISCA is deployed in an aqueous environment, the chemicals diffuse out of the wells through a small

543 port, creating chemical gradients which will guide chemotactic bacteria inside the wells of the
544 device[17,18]. *Vibrio cyclitrophicus* ZF210 was plated on Marine Agar (BD Difco) from a glycerol stock
545 and grown for 16 h at 27 °C. A single colony was then incubated in 10% Marine Broth (BD Difco) in
546 0.22-µm filtered artificial seawater (Instant Ocean, Spectrum Brands) and grown overnight at 27 °C and
547 180 rpm. The culture was diluted down to 1 x 10^6 cells ml^{-1} in 0.22 µm filtered artificial seawater (Instant
548 Ocean, Spectrum Brands) to perform the chemotaxis experiment. Both chemoattractants (alginate and
549 digested alginate) were diluted in sterile seawater (35 g l^{-1}; Instant Ocean, Spectrum Brands) at a final
550 concentration of 0.1% and then filtered with a 0.2 µm filter (Millipore) to remove particles and potential
551 contaminants. Within the ISCA, one full row of five wells was used per chemoattractant as technical
552 replicates. The chemoattractants were injected in triplicate ISCA with a sterile 1 ml syringe (Codau)
553 and needle (27 G, Henke Sass Wolf). A last row containing 0.2 µm-filtered seawater acted as negative
554 control accounting for cells swimming in the device by random motility only. Experiments were
555 conducted by incubating the ISCAs for 1 h in the diluted *Vibrio cyclitrophicus* ZF270 culture. Upon
556 time completion, a sterile syringe and needle were used to retrieve the content of the wells and
557 transferred to 1 ml microfuge tubes resulting in a pooling of a row of 5 wells containing the same
558 sample. Sample staining was performed with SYBR Green I (Thermo Fisher) and the chemotactic
559 response was quantified by counting cells using flow cytometry. The strength of the chemotactic
560 response was determined by the mean chemotactic index (I_C), defined as the ratio of the number of cells
561 found in each chemoattractant to the number of cells in control wells containing filtered seawater (so
562 that attraction corresponds to $I_C > 1$).
563
564 *Culturing and harvesting cells for transcriptomics*
565 Cells were grown for 18 hours in Marine Broth (DIFCO) after which 1 ml of culture was centrifuged at
566 5000 g in 1.5 ml microfuge tubes for 5 minutes. The supernatant was discarded and the cell pellet was
567 subjected to two rounds of washing with the basal TR salts medium. The cell pellet was then
568 resuspended in 1 ml of TR salts medium and 250 µl of this suspension were used to inoculate 100 ml
569 flasks (Schott-Duran) containing 10 ml of TR medium with either 0.1% alginate or 0.1% digested
570 alginate. This was done in parallel for six flasks. Once cultures in the flasks reached mid-exponential

571 phase (10 hours and 15 hours after inoculation for digested alginate and alginate, respectively) and had
572 approximately the same OD (0.39 for digested alginate and 0.41 for alginate), 2 ml of cultures were
573 harvested for RNA extraction. Samples were stabilized with the RNprotect reagent (Qiagen) and RNA
574 was extracted using the RNeasy mini kit (Qiagen).
575
576 *Sequencing and gene annotation of Vibrio cyclitrophicus* ZF270
577 Long read sequencing using the Oxford Nanopore Platform (Long read DNA sequencing kit) and short
578 read sequencing using the Illumina platform (Illumina DNA Prep kit and IDT 10bp UDI indices, and
579 sequenced on an Illumina NextSeq 2000 producing 2x151bp reads) was performed by the Microbial
580 Genome Sequencing Center, Pittsburgh, USA (MiGS), to create a new closed reference genome of *V.*
581 *cyclitrophicus* ZF270 (BioProject PRJNA991487). Annotation of this genome was done with RASTtk
582 (v2.0, Rapid Annotation using Subsystem Technology tool kit[61]). Additionally, KEGG Ontology
583 identifiers ("K numbers") were annotated with BlastKOALA (v2.2)[62]. Dedicated annotation of alginate
584 lyase genes was performed by homology search for proteins belonging to the PL5, PL6, PL7, PL14,
585 PL15, PL17, PL18, PL31, PL36, or PL39 family[63] by dbCAN2 (v9.0)[64]. Enzymes for alginate transport
586 and metabolism were identified by BLASTn-search[65,66] of gene sequences of *Vibrio splendidus* 12B01,
587 which were previously identified as minimum genetic prerequisites for alginate utilization and enabled
588 alginate degradation when cloned into *E. coli*[26].
589
590 *Location prediction of alginate lyases*
591 Signal peptides were annotated using SignalP (v.5.0)[67], and LipoP (v.1.0)[68]. SignalP discriminated
592 between 1) Sec/SPI: "standard" secretory signal peptides transported by the Sec translocon and cleaved
593 by Signal Peptidase I (SPI), 2) Sec/SPII: lipoprotein signal peptides transported by the Sec translocon
594 and cleaved by Signal Peptidase II (SPII), and 3) Tat/SPI: Tat signal peptides transported by the Tat
595 translocon and cleaved by SPI. LipoP discriminates between 1) SPI: signal peptide, 2) SpII: lipoprotein
596 signal peptide, and 3) TMH: n-terminal transmembrane helix. All predictions were in agreement, apart
597 from one PL7 (gene 1136176.5.peg.4375) which was predicted by LipoP as cytoplasmic and by SignalP
598 as equally likely cytoplasmic as containing a lipoprotein signal peptide.

599

600 *Transcriptomic analysis: Sequencing, pre-processing, differential expression analysis, and functional*
601 *analysis*

602 Sequencing (12 M reads, 2 x 50 bp) of the isolated RNA was performed by MiGS after rRNA depletion
603 using RiboZero Plus (Ilumina). cDNA libraries were prepared using an Illumina DNA Prep kit and IDT
604 10 bp UDI indices, and sequenced on an Illumina NextSeq 2000. Preprocessing of the raw reads was
605 carried out as follows: Quality control was performed with FastQC (v0.11.9)[69] and reads were trimmed
606 with Trimmomatic (v0.38)[70]; the high-quality reads were mapped to the reference genome (described
607 above) with Bowtie2 (v2.3.5.1)[71]; binarization, sorting, and indexing were done with Samtools
608 (v1.10)[72]; gene counts were computed with the featureCount function of Subread (v2.0.1)[73].

609 Differential expression analysis was performed with DESeq2 (v1.30.1)[74]. In brief, DESeq2 normalizes
610 the raw read counts with normalization factors ("size factors") to account for differences in sequencing
611 depth between samples. Subsequently, gene-wise dispersion estimates are computed for each gene
612 separately using maximum likelihood, and then shrunk toward the values predicted by the dispersion-
613 mean dependence curve to obtain final dispersion values. Finally, DESeq2 fits a negative binomial
614 model to the read counts and performs significance testing using the Wald test. Here reported *p*-values
615 result from the Wald test of read counts from the digested alginate condition compared to the alginate
616 condition and were adjusted for multiple testing by Benjamini-Hochberg correction[75] as implemented
617 in the p.adjust function of base R (v4.1.2). The reported log2 fold changes indicate the log2(DESeq2-
618 normalised reads in digested alginate condition / DESeq2-normalised reads in alginate condition) for
619 each gene.

620 Visualization of gene maps was performed in R with the ggplot2 package (v3.4.0) and the extension
621 gggenes (v0.4.1) by David Wilkins.

622 For systematic functional analysis we performed gene set enrichment analysis (GSEA)[19] using the fgsea
623 function of the fgsea package (v1.20.0) with minimal number of unique genes per gene set "minSize"
624 = 5 and number of permutations "nPermSimple" = 1000000. In brief, GSEA takes the full gene list
625 ranked by log2 fold change and annotated with K numbers as input and determines whether the member
626 genes of any KEGG pathway are randomly distributed throughout the ranked gene list or whether they

627 are primarily found at the top or bottom[19]. This is quantified by the enrichment score (ES), which
628 corresponds to a weighted Kolmogorov-Smirnov-like statistic. The ES of each gene set is normalized
629 to the mean enrichment of random samples of the same size to account for the size of the set, yielding
630 the normalized enrichment score (NES). To estimate the significance level of the enrichment score, the
631 *p*-value of the observed enrichment score is calculated relative to a null distribution that was computed
632 from permuted data. The estimated significance level was adjusted to account for multiple hypothesis
633 testing. As gene sets we chose all KEGG pathways and KEGG BRITE categories (as noted in Table S1
634 in column "KEGG_pathway") within all genes of *V. cyclitrophicus* ZF270 annotated with a KEGG
635 Ontology identifier ("K number"). Visualization of differential expression levels in KEGG pathways
636 was performed with the R package pathview (v1.35.0)[76]. We also formed gene sets of the genes
637 associated with alginate utilization (see "*Sequencing and gene annotation of Vibrio cyclitrophicus*
638 ZF270", Table S16), of the genes of the flagellar locus that map to the KEGG pathways "Bacterial
639 motility proteins", and of the genes of the flagellar locus that map to the KEGG pathways "Bacterial
640 chemotaxis" (as noted in Table S17) within all genes of *V. cyclitrophicus* ZF270.
641
642 *Image analysis*
643 Cells within microscopy images were segmented and tracked using ilastik (v1.3) ("pixel classification
644 workflow" and "tracking with probabilities workflow"). Phase contrast images were used for alignment,
645 segmentation, tracking and linking. Images were cropped at the boundaries of each microfluidic
646 chamber. The lineage identity of each single cell was assigned by ilastik's tracking plugin and visualized
647 by coloring the segmented cells, respectively. The growth rate of each cell was computed as the change
648 of cell area over time, i.e., via a linear regression of the single-cell area over the time between
649 consecutive cell divisions, based on ilastik's segmentation and tracking output. Cells that were tracked
650 over less than three frames were excluded. Measurement of swimming speeds and displacement of cells
651 was performed using ilastik (v1.4), ImageJ (v2.3) and Trackmate (v7.5.2). Briefly, cell-segmentation
652 ("pixel classification workflow" in ilastik) and tracking ("animal tracking workflow" in ilastik) were
653 performed using the high frame rate phase contrast images in ilastik (v1.4). Cell trajectories and
654 properties were then computed using the output of the ilastik workflow in Trackmate.

655

656 *Dispersal analysis*

657 For the analysis on the dispersal of cells (Fig. 2), we computed the cell number as the total number of
658 cells within a microfluidic chamber. The change in the number of cells was computed by subtracting
659 the number of cells before the medium switch (i.e., average number of cells between t = 1.9 to 2.1 h)
660 from the number of cells after the medium switch (i.e., average number of cells between t = 3.9 to 5.5
661 h).

662

663 *Datasets and statistical analysis*

664 All batch experiments were replicated 3 to 6 times. Growth curves were analyzed in Python (v3.7) using
665 the *Amiga* package (v1.1.0)[77] and GraphPad Prism (v8, GraphPad Software). The microscopy dataset
666 consisted of eight chambers each, corresponding to the eight replicates shown in Figure 1 and Figure 2.
667 These were grouped into two biological replicates wherein each biological replicate was fed by media
668 through a unique channel in a microfluidic chip. Cells with negative growth rates were excluded from
669 the analysis after visual curation, as they represented artefacts, mistakes in segmentation or linking
670 during the tracking process, or non-growing deformed cells. Each chamber was treated as an
671 independent replicate. Comparisons were considered statistically significant when $p < 0.05$ or when the
672 False Discovery Rate (FDR)-corrected q was smaller than 0.05. FDR corrections were applied when
673 multiple t tests were performed for the same dataset. Measures of effect size are represented by the R^2
674 or eta^2 value. All statistical analyses were performed in GraphPad Prism v9.0 (GraphPad Software,
675 USA), R v4.1.2, RStudio v1.1.463 (Posit, USA).

676

677 **Acknowledgements:** We thank past and present members of the Microbial Systems Ecology group for
678 feedback. This research was supported by an ETH fellowship and a Marie Skłodowska-Curie Actions
679 for People COFUND program fellowship (FEL-37-16-1) to GD; an ETH Career Seed Grant to GD
680 (FEL-14 18-1), the Simons Foundation Collaboration on Principles of Microbial Ecosystems (PriME,
681 #542379 and #542395) to MA and RS; and by ETH Zurich and Eawag.

682

Data Availability: Sequencing data is available on NCBI, BioProject PRJNA991487, upon publication. All further data is deposited on ERIC Open (https://opendata.eawag.ch/, https://doi.org/10.25678/0008MH), available upon publication. All code will be made publicly accessible on https://github.com/Microbial-Systems-Ecology/publications upon publication.

Competing interests: The authors declare no competing interests.

Author Contributions: GD, AS, JS, and JK conceived the research along with MA. GD designed and performed the experiments. AS developed and implemented the algorithms to compute single-cell growth rates and visualize lineage identities from segmented and tracked cells. AS analyzed and visualized the RNA-seq data. JK conceived and implemented the cell dispersal analysis. EC conducted the ISCA experiment. SP carried out the mass spectrometry measurements. AS and GD analyzed the data with inputs from JK, JS, CM, MA, and RS. AS wrote the manuscript with inputs from GD, OS, MA, JK, JS, EC, SP, CM, and RS.

Citations:

1. BeMiller JN. 4 - Polysaccharides: Occurrence, Structures, and Chemistry. In: BeMiller JN, ed. *Carbohydrate Chemistry for Food Scientists (Third Edition)*. AACC International Press; 2019:75-101. doi:10.1016/B978-0-12-812069-9.00004-2

2. Reintjes G, Arnosti C, Fuchs B, Amann R. Selfish, sharing and scavenging bacteria in the Atlantic Ocean: a biogeographical study of bacterial substrate utilisation. *ISME J*. 2019;13(5):1119-1132. doi:10.1038/s41396-018-0326-3

3. Ratzke C, Gore J. Self-organized patchiness facilitates survival in a cooperatively growing Bacillus subtilis population. *Nature Microbiology*. 2016;1(5):16022. doi:10.1038/nmicrobiol.2016.22

4. Povolo VR, D'Souza GG, Kaczmarczyk A, Stubbusch AK, Jenal U, Ackermann M. Extracellular appendages govern spatial dynamics and growth of Caulobacter crescentus on a prevalent biopolymer. *bioRxiv*. Published online January 1, 2022:2022.06.13.495907. doi:10.1101/2022.06.13.495907

5. Westrich JR, Griffin DW, Westphal DL, Lipp EK. Vibrio Population Dynamics in Mid-Atlantic Surface Waters during Saharan Dust Events. *Frontiers in Marine Science*. 2018;5. https://www.frontiersin.org/articles/10.3389/fmars.2018.00012

715 6. Takemura A, Chien D, Polz M. Associations and dynamics of Vibrionaceae in the environment,
716 from the genus to the population level. *Frontiers in Microbiology*. 2014;5.
717 https://www.frontiersin.org/articles/10.3389/fmicb.2014.00038

718 7. Schwartzman JA, Ebrahimi A, Chadwick G, Sato Y, Orphan V, Cordero OX. Bacterial growth in
719 multicellular aggregates leads to the emergence of complex lifecycles. *bioRxiv*. Published online
720 January 1, 2021:2021.11.01.466752. doi:10.1101/2021.11.01.466752

721 8. D'Souza G, Ebrahimi A, Stubbusch A, et al. Cell aggregation is associated with enzyme secretion
722 strategies in marine polysaccharide-degrading bacteria. *ISME J*. Published online February 22,
723 2023. doi:10.1038/s41396-023-01385-1

724 9. Wang X, Liu J, Liang J, Sun H, Zhang XH. Spatiotemporal dynamics of the total and active Vibrio
725 spp. populations throughout the Changjiang estuary in China. *Environmental Microbiology*.
726 2020;22(10):4438-4455. doi:10.1111/1462-2920.15152

727 10. Mabeau S, Kloareg B. Isolation and Analysis of the Cell Walls of Brown Algae: Fucus
728 spiralis, F. ceranoides, F. vesiculosus, F. serratus, Bifurcaria bifurcata and Laminaria digitata.
729 *Journal of Experimental Botany*. 1987;38(9):1573-1580. doi:10.1093/jxb/38.9.1573

730 11. Wong TY, Preston LA, Schiller NL. Alginate Lyase: Review of Major Sources and Enzyme
731 Characteristics, Structure-Function Analysis, Biological Roles, and Applications. *Annual Review of*
732 *Microbiology*. 2000;54(1):289-340. doi:10.1146/annurev.micro.54.1.289

733 12. Hunt DE, David LA, Gevers D, Preheim SP, Alm EJ, Polz MF. Resource Partitioning and
734 Sympatric Differentiation Among Closely Related Bacterioplankton. *Science*. Published online
735 May 23, 2008. doi:10.1126/science.1157890

736 13. Yawata Y, Cordero OX, Menolascina F, Hehemann JH, Polz MF, Stocker R. Competition–
737 dispersal tradeoff ecologically differentiates recently speciated marine bacterioplankton
738 populations. *Proc Natl Acad Sci USA*. 2014;111(15):5622-5627. doi:10.1073/pnas.1318943111

739 14. D'Souza GG, Povolo VR, Keegstra JM, Stocker R, Ackermann M. Nutrient complexity
740 triggers transitions between solitary and colonial growth in bacterial populations. *ISME J*.
741 2021;15(9):2614-2626. doi:10.1038/s41396-021-00953-7

742 15. Huang L, Zhou J, Li X, Peng Q, Lu H, Du Y. Characterization of a new alginate lyase from
743 newly isolated *Flavobacterium* sp. S20. *Journal of Industrial Microbiology and Biotechnology*.
744 2013;40(1):113-122. doi:10.1007/s10295-012-1210-1

745 16. Dal Co A, van Vliet S, Kiviet DJ, Schlegel S, Ackermann M. Short-range interactions govern
746 the dynamics and functions of microbial communities. *Nat Ecol Evol*. 2020;4(3):366-375.
747 doi:10.1038/s41559-019-1080-2

748 17. Lambert BS, Raina JB, Fernandez VI, et al. A microfluidics-based in situ chemotaxis assay to
749 study the behaviour of aquatic microbial communities. *Nat Microbiol*. 2017;2(10):1344-1349.
750 doi:10.1038/s41564-017-0010-9

751 18. Clerc EE, Raina JB, Lambert BS, Seymour J, Stocker R. In Situ Chemotaxis Assay to
752 Examine Microbial Behavior in Aquatic Ecosystems. *JoVE*. 2020;(159):e61062.
753 doi:10.3791/61062

754 19. Subramanian A, Tamayo P, Mootha VK, et al. Gene set enrichment analysis: a knowledge-
755 based approach for interpreting genome-wide expression profiles. *Proc Natl Acad Sci U S A*.
756 2005;102(43):15545-15550. doi:10.1073/pnas.0506580102

757 20. Wei Y, Lee JM, Richmond C, Blattner FR, Rafalski JA, LaRossa RA. High-Density
758 Microarray-Mediated Gene Expression Profiling of *Escherichia coli*. *J Bacteriol*. 2001;183(2):545-
759 556. doi:10.1128/JB.183.2.545-556.2001

760 21. Gifford SM, Sharma S, Booth M, Moran MA. Expression patterns reveal niche diversification
761 in a marine microbial assemblage. *ISME J*. 2013;7(2):281-298. doi:10.1038/ismej.2012.96

762 22. Johnson TL, Fong JC, Rule C, Rogers A, Yildiz FH, Sandkvist M. The Type II Secretion
763 System Delivers Matrix Proteins for Biofilm Formation by Vibrio cholerae. *J Bacteriol*.
764 2014;196(24):4245-4252. doi:10.1128/JB.01944-14

765 23. Sikora AE. Proteins Secreted via the Type II Secretion System: Smart Strategies of Vibrio
766 cholerae to Maintain Fitness in Different Ecological Niches. Heitman J, ed. *PLoS Pathog*.
767 2013;9(2):e1003126. doi:10.1371/journal.ppat.1003126

768 24. Jemielita M, Wingreen NS, Bassler BL. Quorum sensing controls Vibrio cholerae
769 multicellular aggregate formation. Storz G, ed. *eLife*. 2018;7:e42057. doi:10.7554/eLife.42057

770 25. Waters CM, Lu W, Rabinowitz JD, Bassler BL. Quorum sensing controls biofilm formation
771 in Vibrio cholerae through modulation of cyclic di-GMP levels and repression of vpsT. *J Bacteriol*.
772 2008;190(7):2527-2536. doi:10.1128/JB.01756-07

773 26. Wargacki AJ, Leonard E, Win MN, et al. An Engineered Microbial Platform for Direct
774 Biofuel Production from Brown Macroalgae. *Science*. Published online January 20, 2012.
775 doi:10.1126/science.1214547

776 27. Zhang L, Li X, Zhang X, Li Y, Wang L. Bacterial alginate metabolism: an important pathway
777 for bioconversion of brown algae. *Biotechnol Biofuels*. 2021;14(1):158. doi:10.1186/s13068-021-
778 02007-8

779 28. Khan F, Tabassum N, Anand R, Kim YM. Motility of Vibrio spp.: regulation and controlling
780 strategies. *Appl Microbiol Biotechnol*. 2020;104(19):8187-8208. doi:10.1007/s00253-020-10794-7

781 29. Echazarreta MA, Klose KE. Vibrio Flagellar Synthesis. *Front Cell Infect Microbiol*.
782 2019;9:131. doi:10.3389/fcimb.2019.00131

783 30. Prouty MG, Correa NE, Klose KE. The novel sigma54- and sigma28-dependent flagellar gene
784 transcription hierarchy of Vibrio cholerae. *Mol Microbiol*. 2001;39(6):1595-1609.
785 doi:10.1046/j.1365-2958.2001.02348.x

786 31. Klose KE, Mekalanos JJ. Differential Regulation of Multiple Flagellins in *Vibrio cholerae*. *J*
787 *Bacteriol*. 1998;180(2):303-316. doi:10.1128/JB.180.2.303-316.1998

788 32. Srivastava D, Hsieh ML, Khataokar A, Neiditch MB, Waters CM. Cyclic di-GMP inhibits
789 Vibrio cholerae motility by repressing induction of transcription and inducing extracellular
790 polysaccharide production. *Mol Microbiol*. 2013;90(6):1262-1276. doi:10.1111/mmi.12432

791 33. Kim SY, Thanh XTT, Jeong K, et al. Contribution of six flagellin genes to the flagellum
792 biogenesis of Vibrio vulnificus and in vivo invasion. *Infect Immun*. 2014;82(1):29-42.
793 doi:10.1128/iai.00654-13

794 34. Nedeljković M, Sastre DE, Sundberg EJ. Bacterial Flagellar Filament: A Supramolecular
795 Multifunctional Nanostructure. *Int J Mol Sci*. 2021;22(14):7521. doi:10.3390/ijms22147521

35. Rajagopala SV, Titz B, Goll J, et al. The protein network of bacterial motility. *Mol Syst Biol*. 2007;3(1):128. doi:10.1038/msb4100166

36. Ebrahimi A, Schwartzman J, Cordero OX. Cooperation and spatial self-organization determine rate and efficiency of particulate organic matter degradation in marine bacteria. *Proc Natl Acad Sci USA*. 2019;116(46):23309-23316. doi:10.1073/pnas.1908512116

37. Drescher K, Nadell CD, Stone HA, Wingreen NS, Bassler BL. Solutions to the Public Goods Dilemma in Bacterial Biofilms. *Current Biology*. 2014;24(1):50-55. doi:10.1016/j.cub.2013.10.030

38. Alcolombri U, Peaudecerf FJ, Fernandez VI, Behrendt L, Lee KS, Stocker R. Sinking enhances the degradation of organic particles by marine bacteria. *Nat Geosci*. 2021;14(10):775-780. doi:10.1038/s41561-021-00817-x

39. Yawata Y, Carrara F, Menolascina F, Stocker R. Constrained optimal foraging by marine bacterioplankton on particulate organic matter. *Proc Natl Acad Sci USA*. 2020;117(41):25571-25579. doi:10.1073/pnas.2012443117

40. McDougald D, Rice SA, Barraud N, Steinberg PD, Kjelleberg S. Should we stay or should we go: mechanisms and ecological consequences for biofilm dispersal. *Nat Rev Microbiol*. 2012;10(1):39-50. doi:10.1038/nrmicro2695

41. Thomas F, Barbeyron T, Tonon T, Génicot S, Czjzek M, Michel G. Characterization of the first alginolytic operons in a marine bacterium: from their emergence in marine Flavobacteriia to their independent transfers to marine Proteobacteria and human gut Bacteroides: Emergence and transfer of alginolytic operons. *Environmental Microbiology*. 2012;14(9):2379-2394. doi:10.1111/j.1462-2920.2012.02751.x

42. Dudek M, Dieudonné A, Jouanneau D, et al. Regulation of alginate catabolism involves a GntR family repressor in the marine flavobacterium Zobellia galactanivorans DsijT. *Nucleic Acids Research*. 2020;48(14):7786-7800. doi:10.1093/nar/gkaa533

43. Guessous G, Patsalo V, Balakrishnan R, Çağlar T, Williamson JR, Hwa T. Inherited chitinases enable sustained growth and rapid dispersal of bacteria from chitin particles. *Nat Microbiol*. 2023;8(9):1695-1705. doi:10.1038/s41564-023-01444-5

44. Chubukov V, Gerosa L, Kochanowski K, Sauer U. Coordination of microbial metabolism. *Nat Rev Microbiol*. 2014;12(5):327-340. doi:10.1038/nrmicro3238

45. Martínez-Antonio A, Janga SC, Salgado H, Collado-Vides J. Internal-sensing machinery directs the activity of the regulatory network in Escherichia coli. *Trends in Microbiology*. 2006;14(1):22-27. doi:10.1016/j.tim.2005.11.002

46. Bassler BL, Gibbons PJ, Yu C, Roseman S. Chitin utilization by marine bacteria. Chemotaxis to chitin oligosaccharides by Vibrio furnissii. *Journal of Biological Chemistry*. 1991;266(36):24268-24275. doi:10.1016/S0021-9258(18)54224-1

47. Meibom KL, Li XB, Nielsen AT, Wu CY, Roseman S, Schoolnik GK. The *Vibrio cholerae* chitin utilization program. *Proc Natl Acad Sci USA*. 2004;101(8):2524-2529. doi:10.1073/pnas.0308707101

48. Mandel MJ, Schaefer AL, Brennan CA, et al. Squid-Derived Chitin Oligosaccharides Are a Chemotactic Signal during Colonization by Vibrio fischeri. *Appl Environ Microbiol*. 2012;78(13):4620-4626. doi:10.1128/AEM.00377-12

837 49. Purcell EM. Life at low Reynolds number. *American Journal of Physics*. 1977;45(1):3-11.
838 doi:10.1119/1.10903

839 50. Blackburn N, Fenchel T, Mitchell J. Microscale Nutrient Patches in Planktonic Habitats
840 Shown by Chemotactic Bacteria. *Science*. 1998;282(5397):2254-2256.
841 doi:10.1126/science.282.5397.2254

842 51. Blackburn N, Fenchel T. Influence of bacteria, diffusion and shear on micro-scale nutrient
843 patches, and implications for bacterial chemotaxis. *Mar Ecol Prog Ser*. 1999;189:1-7.
844 doi:10.3354/meps189001

845 52. Fenchel T. Microbial Behavior in a Heterogeneous World. *Science*. 2002;296(5570):1068-
846 1071. doi:10.1126/science.1070118

847 53. Smriga S, Fernandez VI, Mitchell JG, Stocker R. Chemotaxis toward phytoplankton drives
848 organic matter partitioning among marine bacteria. *Proc Natl Acad Sci USA*. 2016;113(6):1576-
849 1581. doi:10.1073/pnas.1512307113

850 54. Ronce O. How Does It Feel to Be Like a Rolling Stone? Ten Questions About Dispersal
851 Evolution. *Annu Rev Ecol Evol Syst*. 2007;38(1):231-253.
852 doi:10.1146/annurev.ecolsys.38.091206.095611

853 55. Fenchel T. Motility of bacteria in sediments. *Aquat Microb Ecol*. 2008;51:23-30.
854 doi:10.3354/ame01182

855 56. Rumbaugh KP, Sauer K. Biofilm dispersion. *Nat Rev Microbiol*. 2020;18(10):571-586.
856 doi:10.1038/s41579-020-0385-0

857 57. Hehemann JH, Arevalo P, Datta MS, et al. Adaptive radiation by waves of gene transfer leads
858 to fine-scale resource partitioning in marine microbes. *Nat Commun*. 2016;7:12860.
859 doi:10.1038/ncomms12860

860 58. Tibbles BJ, Rawlings DE. Characterization of nitrogen-fixing bacteria from a temperate
861 saltmarsh lagoon, including isolates that produce ethane from acetylene. *Microb Ecol*. 1994;27(1).
862 doi:10.1007/BF00170115

863 59. D'Souza G, Waschina S, Pande S, Bohl K, Kaleta C, Kost C. Less is more: Selective
864 advantages can explain the prevalent loss of biosynthetic genes in bacteria. *Evolution*.
865 2014;68(9):2559-2570. doi:10.1111/evo.12468

866 60. Mathis R, Ackermann M. Response of single bacterial cells to stress gives rise to complex
867 history dependence at the population level. *Proc Natl Acad Sci USA*. 2016;113(15):4224-4229.
868 doi:10.1073/pnas.1511509113

869 61. Brettin T, Davis JJ, Disz T, et al. RASTtk: A modular and extensible implementation of the
870 RAST algorithm for building custom annotation pipelines and annotating batches of genomes. *Sci*
871 *Rep*. 2015;5(1):8365. doi:10.1038/srep08365

872 62. Kanehisa M, Sato Y, Morishima K. BlastKOALA and GhostKOALA: KEGG Tools for
873 Functional Characterization of Genome and Metagenome Sequences. *Journal of Molecular*
874 *Biology*. 2016;428(4):726-731. doi:10.1016/j.jmb.2015.11.006

875 63. Cheng D, Jiang C, Xu J, Liu Z, Mao X. Characteristics and applications of alginate lyases: A
876 review. *International Journal of Biological Macromolecules*. 2020;164:1304-1320.
877 doi:10.1016/j.ijbiomac.2020.07.199

878 64. Zhang H, Yohe T, Huang L, et al. dbCAN2: a meta server for automated carbohydrate-active
879 enzyme annotation. *Nucleic Acids Res*. 2018;46(W1):W95-W101. doi:10.1093/nar/gky418

880 65. NCBI Resource Coordinators. Database resources of the National Center for Biotechnology
881 Information. *Nucleic Acids Res*. 2016;44(Database issue):D7-D19. doi:10.1093/nar/gkv1290

882 66. Altschul SF, Gish W, Miller W, Myers EW, Lipman DJ. Basic local alignment search tool. *J*
883 *Mol Biol*. 1990;215(3):403-410. doi:10.1016/S0022-2836(05)80360-2

884 67. Almagro Armenteros JJ, Tsirigos KD, Sønderby CK, et al. SignalP 5.0 improves signal
885 peptide predictions using deep neural networks. *Nat Biotechnol*. 2019;37(4):420-423.
886 doi:10.1038/s41587-019-0036-z

887 68. Juncker AS, Willenbrock H, von Heijne G, Brunak S, Nielsen H, Krogh A. Prediction of
888 lipoprotein signal peptides in Gram-negative bacteria. *Protein Sci*. 2003;12(8):1652-1662.

889 69. Andrews S. FastQC: A Quality Control Tool for High Throughput Sequence Data [Online].
890 Available online at: http://www.bioinformatics.babraham.ac.uk/projects/fastqc/. Published online
891 2010. http://www.bioinformatics.babraham.ac.uk/projects/fastqc/

892 70. Bolger AM, Lohse M, Usadel B. Trimmomatic: a flexible trimmer for Illumina sequence data.
893 *Bioinformatics*. 2014;30(15):2114-2120. doi:10.1093/bioinformatics/btu170

894 71. Langmead B, Salzberg SL. Fast gapped-read alignment with Bowtie 2. *Nat Methods*.
895 2012;9(4):357-359. doi:10.1038/nmeth.1923

896 72. Danecek P, Bonfield JK, Liddle J, et al. Twelve years of SAMtools and BCFtools.
897 *Gigascience*. 2021;10(2):giab008. doi:10.1093/gigascience/giab008

898 73. Liao Y, Smyth GK, Shi W. featureCounts: an efficient general purpose program for assigning
899 sequence reads to genomic features. *Bioinformatics*. 2014;30(7):923-930.
900 doi:10.1093/bioinformatics/btt656

901 74. Love MI, Huber W, Anders S. Moderated estimation of fold change and dispersion for RNA-
902 seq data with DESeq2. *Genome Biology*. 2014;15(12):550. doi:10.1186/s13059-014-0550-8

903 75. Benjamini Y, Hochberg Y. Controlling the False Discovery Rate: A Practical and Powerful
904 Approach to Multiple Testing. *Journal of the Royal Statistical Society: Series B (Methodological)*.
905 1995;57(1):289-300. doi:10.1111/j.2517-6161.1995.tb02031.x

906 76. Luo W, Brouwer C. Pathview: an R/Bioconductor package for pathway-based data integration
907 and visualization. *Bioinformatics*. 2013;29(14):1830-1831. doi:10.1093/bioinformatics/btt285

908 77. Midani FS, Collins J, Britton RA. AMiGA: Software for Automated Analysis of Microbial
909 Growth Assays. Silva-Rocha R, ed. *mSystems*. 2021;6(4):e00508-21.
910 doi:10.1128/mSystems.00508-21

911